
Airflow in the Ventilation Space Behind a Rain Screen Wall

Therese K. Stovall, P.E.
Member ASHRAE

Achilles Karagiozis, Ph.D.

ABSTRACT

The inclusion of a ventilated airspace within a wall has been shown to improve the moisture transport of the wall assembly. Experimental data describing the airflow within such a cavity are available for a limited range of weather conditions and geometric configurations, but general relationships between the ventilation within the wall and external weather variables are not. Therefore, a series of steady-state numerical models was constructed to explore the influence of weather variables, including wind speed, insolation, and outdoor air temperature, for brick rain screen wall configurations. These configurations included multiple cavity depths and vent sizes. All models were based on a single-story building height with wind perpendicular to the wall. The results were used to develop a number of correlations intended to supplement the accuracy of transient hygrothermal models.

INTRODUCTION

The inclusion of a ventilated airspace within a wall has been shown to improve the moisture transport of the wall assembly. The purpose of the analysis reported here was to produce general relationships that describe the airflow through a rain screen wall configuration in terms of weather variables and ventilation cavity geometry. These correlations were intended to supplement one- and two-dimensional transient hygrothermal models. The effects of increasing the cavity depth and ventilation opening size were of particular interest.

Vent and ventilation research has primarily focused on pressure equalization analysis, and only limited data are found that include the effects of moisture management. Most of the past work including integrated heat, air, and moisture transfer is found in Europe. An excellent summary of work in this field has just been prepared by Straube (2004).

Experimental data describing the airflow within such a cavity are available for a limited range of weather conditions and geometric configurations. Schwarz (1973) measured the velocity of the airflow in an open-jointed panel cladding system in a high-rise building. He found little relationship

between building height and cavity ventilation velocity. Popp et al. (1980) measured the ventilation velocity and air exchange rate behind asbestos cement and wood siding with various types of cavities and venting arrangements. It was clear the drying rate was much faster when the cladding was ventilated, although even simple venting (small openings through the cladding without a clear airflow space behind) improved the drying rate. Another project included field measurements of ventilation behind large cladding panels on a three-story building (Mayer and Kuenzel 1983; Kuenzel and Mayer 1983, 1984 [as quoted by Straube (2004)]). Burnett and Straube (1995) conducted an experimental study of the flow resistance of vents and made detailed field measurements of wind-driving pressures. Transient pressure measurements were made for a rain screen façade, capturing the effect of variable wind conditions for a relatively tall building (Kumar and Wisse 2001; Kumar et al. 2003). Hansen et al. (2002) performed a field study of ventilating cavities in timber-framed wall assemblies, including 12 different wall assemblies with various types of cladding and wind barriers and ventilated/nonventilated spaces and space/no space combinations. The authors concluded that ventilation had no signifi-

Therese K. Stovall and **Achilles Karagiozis** are senior research engineers at Oak Ridge National Laboratory, Oak Ridge, Tenn.

cant moisture control influence on timber-framed wall systems. Recent experimental work on brick rain screen configurations includes that of Straube (1998) and Piñon et al. (2004). These experiments provide an essential foundation for all of the related analyses and simulations. In particular, the work by Mayer, Kuenzel, Straube, Burnett, and Piñon showed that the most important factors for determining the ventilation flow rate were the wind pressure, thermal buoyancy, presence of an unobstructed cavity, and vent area.

A number of pertinent analytical works complement these experimental resources. One study was a theoretical analysis of the flow mechanics and drying physics of ventilation (Burnett and Straube 1995). Further analysis showed that air flows through ventilation spaces due to the combined effects of wind pressure, thermal buoyancy, and moisture concentration buoyancy (Straube 1998). Other analysts have addressed a number of issues pertinent to this geometry. The effect of discrete rough elements, such as could be caused by protruding mortar joints, has been modeled for an enclosure by Shakerin et al. (1988). A finite element model for a more completely ventilated façade has been reported by Balocco (2001). A numerical model and related experiments for a rain screen façade with a flexible back layer were reported by Choi and Wang (1998). Recent work by Piñon et al. (2004) includes an isothermal CFD model of a brick wall with a vent arrangement very similar to the one used here.

Recognizing that it is not feasible to experimentally measure the performance for every wall configuration in every possible climate, one- and two-dimensional hygrothermal analysis tools have been developed. These tools evaluate the transient moisture performance of buildings over an extended period using weather data for a variety of climates and physical models of moisture storage and transport within the wall components (Karagiozis 2001). However, these hygrothermal porous models usually employ Darcy's equation for porous media and are thus unable to properly model the critical drying capabilities that result from the convective movement of air within the ventilation cavity. Therefore, air movements within a wall ventilation cavity caused by thermal buoyancy and wind forces were examined in detail using computational fluid dynamics (CFD) tools more suited for such analysis. After the CFD results were benchmarked via comparison to the available empirical data, the results were then correlated to weather parameters and construction details in order to supplement these broader hygrothermal analysis tools.

MODEL CONSTRUCTION

The wall structure considered here was a nominal 2×4 wood-framed wall with gypsum drywall on the inside, insulated with glass fiber batt insulation, sheathed with a layer of building paper, and finished with a brick veneer on the outside. A ventilated wall cavity was located between the building paper surface and the brick veneer, as shown in Figure 1. The vents shown in this figure were each the size of a typical vertical mortar joint between bricks and were placed in vertical

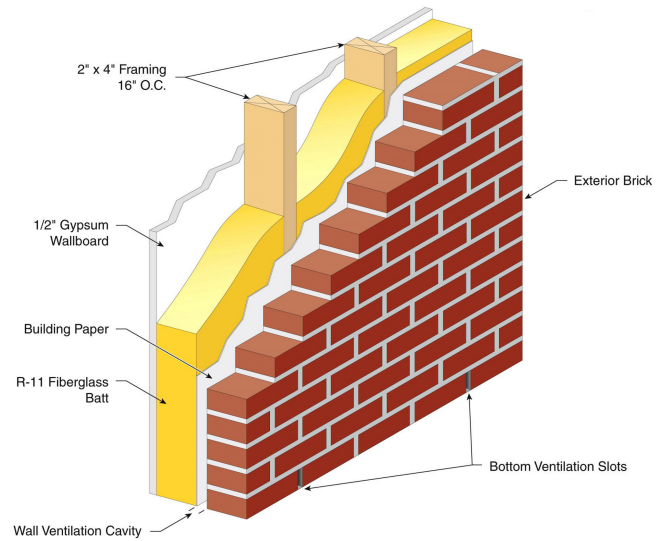


Figure 1 Brick veneer wall.

pairs at a spacing that corresponds to a pair of vents placed after every third brick.

The basic model geometry, shown in Figure 2, consisted of the following layers: external free air, the brick rain screen, an air cavity, and an internal composite wall. The overall height was 2.43 m, and the depth of the outside free airspace was 0.5 m. The inclusion of an external air volume allowed the pressure to vary over the surface of the brick wall (and, therefore, at the ventilation slots), reflecting stagnation conditions that varied with the local air velocity. The air entered this external air volume through the face opposite the brick wall in a direction normal to the wall. The brick was 0.116 m thick. Vents connecting the external free air and the air cavity within the wall were placed at ground level and 0.070 m from the top of the brick wall. Each vent was 0.009 m wide by 0.079 m high. (The thickness of the vent inlet and outlet slots is shown as 0.0045 m in Figure 2 because a plane of symmetry bounding the model runs through the center of these slots.) Larger vents corresponding to the height of two courses of brick (0.009 m wide by 0.158 m high) were also modeled. The air cavity depth was set to either 0.050 or 0.019 m. The internal composite wall shown in Figure 2 represented the combination of gypsum wallboard, wood framing, insulation, and building paper, and it was 0.1 m thick.

Assumptions

Given the limited temperature and pressure ranges of this investigation, all material and fluid properties were held constant, as shown in Table 1. All analyses were steady state.

Because the focus of this investigation was on the air movement within the cavity, no attempt was made to model the individual components of the interior wall. This wall was therefore assumed homogenous, with the properties shown in

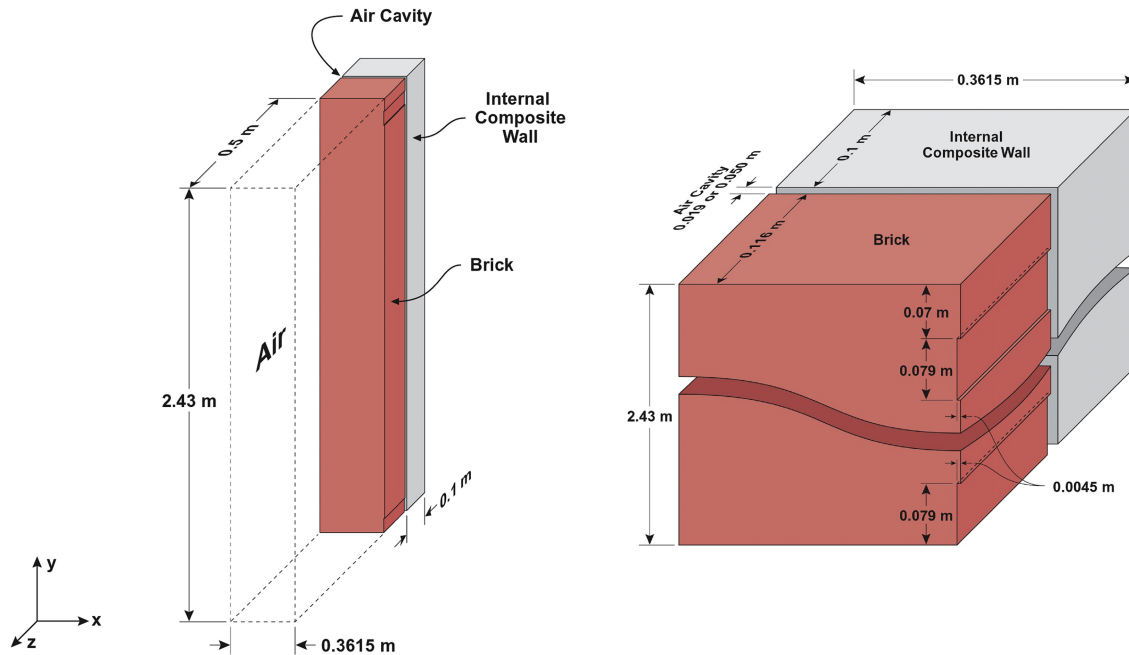


Figure 2 Geometry of the simulated brick veneer wall, close-up view of the ventilation slots on right.

Table 1. Material Properties

	Thermal Conductivity (W/m·K)	Density (kg/m ³)	Specific Heat (J/kg·K)	Dynamic Viscosity (kg/m·s)	Thermal Expansivity (1/K)
Brick wall	0.9	1920.0	790.0		
Internal composite wall	0.056	158.0	1300.0		
Dry air	0.0243	1.284	1003.8	1.72E-5	0.00367

Table 1. The surface of this wall opposite the ventilation cavity was assumed to face a 295 K indoor environment with a natural convection heat transfer coefficient on that surface of 8.3 W/m²·K.

The nonuniformities of bricks and mortar joints are highly variable and were not modeled. However, two air cavity depths were evaluated—0.050 and 0.019 m—to investigate the impact of flow restrictions.

Planes of symmetry were used at each side within the thin cavity and for the sides of the brick and interior walls to represent a relatively narrow section of a longer wall with ordered vent spacing. The top and bottom of the air cavity were modeled as adiabatic smooth walls. The external air volume was bounded by a plane of symmetry on one side (which also passed through the vent holes in the brick wall), an opening at the other side with a constant relative pressure of 0 Pa, and an opening at the top with the relative pressure set to either 0 or 2 Pa. This arrangement represents a wall section near the center of a much longer wall. The bottom of the external air volume was assumed to be a smooth adiabatic surface.

The thermal buoyancy-driven flows were modeled using the Boussinesq approximation with constant density air. This approximation adds a buoyancy momentum term to the equation that is a function of the fluid’s thermal expansivity and temperature (Kays and Crawford 1980; AEA Technology Engineering Software Ltd.).

Examination of local Reynolds numbers, as well as experimental data reported by Piñon et al. (2004), showed transitional and laminar flows in some portions of the air cavity. Results from the CFD model showed minimum Reynolds numbers ranging from 50 to 350 within the main portion of the cavity. Reynolds numbers within the ventilation slots ranged from 600 to 5500. However, significant regions of separated and recirculating flow are also present because of the complex geometry that includes sharp inlets, outlets, and elbows. The turbulence approximation selected for this model uses local terms calculated for turbulence kinetic energy and turbulence eddy dissipation (which varied by a factor of 1000 or more from one portion of the cavity to another) to reflect this variability in flow characteristics. That is, in the laminar flow regions, the turbulence energy factors become very small.

Table 2. Parametric Case Summary

Case ID	Wind Velocity Normal to Wall (m/s)	Outside Air Temperature (K)	Solar Radiation on Wall (W/m ²)	Height of Ventilation Slots (mm)	Ventilation Cavity Depth (mm)
W1	0	250	630	79	50
W2	1	250	630	79	50
W3	4	250	0	79	50
W4	4	250	0	79	19
W5	4	250	630	79	50
W6	4	250	630	79	19
W7	4	250	910	79	50
W8	10	250	630	79	50
S1	0	305	630	79	50
S2	1	305	630	79	50
S3	1	305	630	79	50
S4	1	305	630	79	19
S5	4	305	0	79	50
S6	4	305	0	79	19
S7	4	305	630	79	50
S8	4	305	630	79	19
S9	4	305	630	158	50
S10	4	305	630	158	19
S11	4	305	910	79	50
S12	7	305	630	79	50
S13	10	305	630	79	50

To simulate the absorption of solar energy, a uniform energy source was placed within a thin layer of the brick wall along the surface facing the exterior airspace. This arrangement permits the local temperature to be determined by the combination of three-dimensional heat conduction throughout the brick wall and the convective heat transfer conditions on each surface of the wall.

Organization of the Parametric Evaluation

The ultimate goal of this investigation was to produce simple correlations that describe the airflow through the ventilation cavity in terms of weather variables and cavity geometry. The airflow is characterized by the pressure drops through the inlet and outlet ventilation slots, the pressure variation within the cavity, the flow rate of air through the cavity, and the flow patterns within the cavity. These factors were examined using the matrix of case models shown in Table 2. This matrix permits an examination of the individual contribution of each parameter, covering five wind speeds, two outdoor air temperatures, three levels of solar radiation, two slot heights, and two cavity depths. For example, Cases S1, S2, S7, S12, and S13 are identical in all respects except the wind velocity. Cases S7-S10 compare ventilation slot height variations for two different

cavity depths while keeping all other variables constant. There are seven pairs of cases where all variables were the same except for cavity depth. Eight pairs match every variable except outdoor air temperature.

Limitations

There are, of course, limitations to this work. Air diffusion through the bricks, air leakage through the interior wall, mortar protrusions, and cavity blockages were not modeled. All wall surfaces were considered smooth. The steady-state CFD model does not capture the transient effect of wind speed perturbations. Only dry air was considered in these models, so the additional buoyancy due to variations in moisture content throughout the height of the cavity was not reflected in the results. Radiant heat transfer within the ventilation cavity was not modeled. Although the ventilation opening height was varied, the horizontal and vertical spacing between openings was not. The only wind direction included here was normal to the wall. This last factor may be important in light of experimental work that showed wind direction to have a greater influence on the ventilation airflow than wind speed, although the geometry for those measurements is not known (Kuenzel and Mayer 1983 [as quoted in Straube (2004)]).

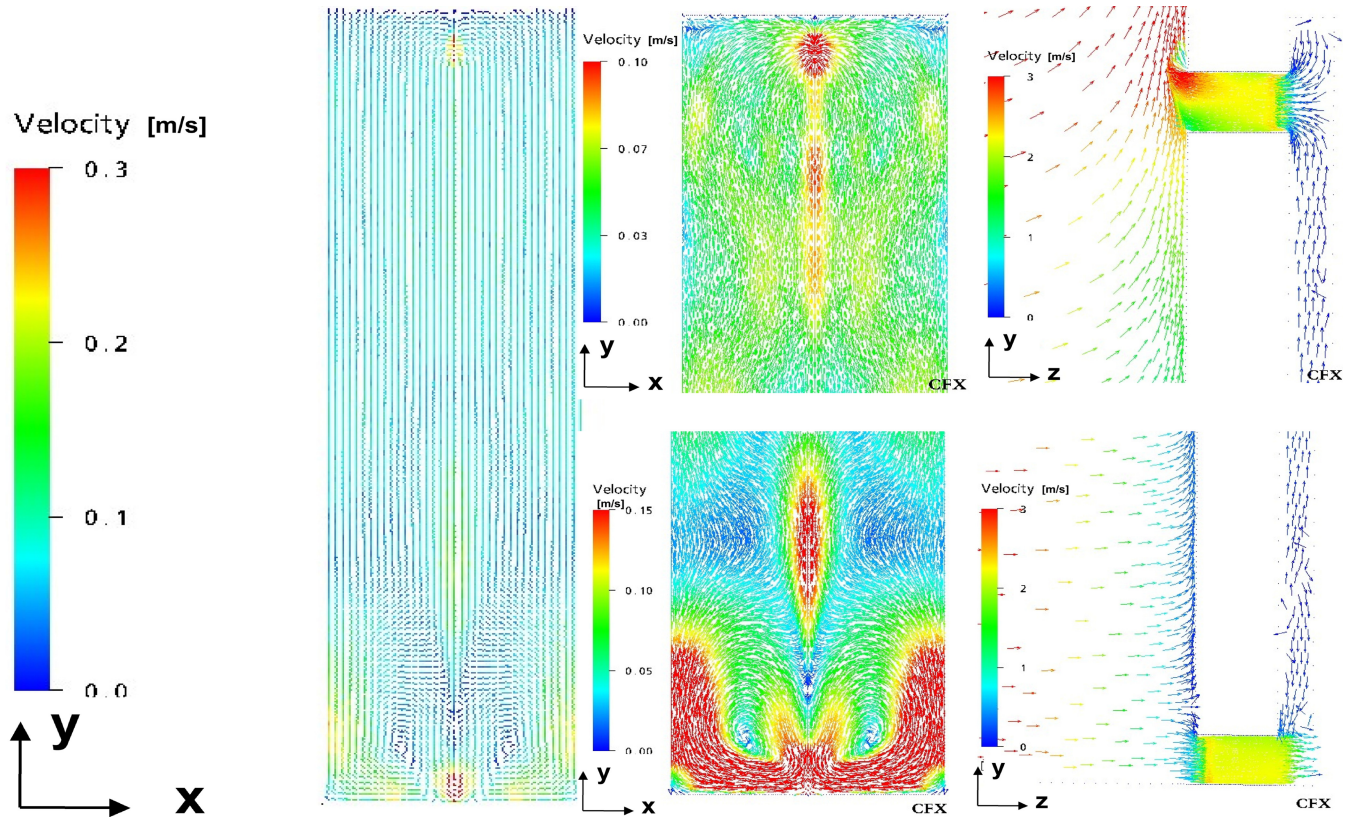


Figure 3 Clockwise, starting left, all from Case S7: Velocity field midway between the brick and building paper surfaces of the cavity, mirrored about the plane of symmetry; close-up view near the top ventilation slot; close-up side view near the top ventilation slot; close-up side view near the bottom ventilation slot; close-up view near the bottom ventilation slot.

MODEL VALIDATION

The CFD model was validated by comparison to experimental data. The points of comparison include flow field visualization, temperature differences, pressure drops, and airflow rates.

Flow Field Visualization

A typical velocity field on a plane through the center of the cavity is shown in Figure 3. For most cases, air flowed in at the bottom opening and out at the top. A localized low-pressure region, present where air entered the cavity at the bottom ventilation slot, tended to pull air in the cavity downward, producing a strong recirculation region directly above the slot. Local regions of recirculation are also evident along the top of the cavity midway between ventilation slots (along the planes of symmetry). Figure 3 includes close-up views of the velocity field in the upper and lower portions of the cavity. The recirculation at the top of the cavity was much less than that near the bottom. Experimental work with a smoke pencil, using a plate of Plexiglas to represent a brick wall, found a very similar flow pattern (Piñon et al. 2004). This same set of experiments also included a brick wall cavity, constructed with and without mortar protrusions. Velocity measurements using that appara-

tus also show that backflow directly above the bottom slot occurs for the brick wall but is somewhat reduced by the regular pattern of horizontal protrusions on the brick wall surface as compared to the smooth Plexiglas surface.

Thermal Comparisons

Empirical data show a maximum brick wall temperature of about 325 K (Straube and Burnett 1998a). Although the empirical data do not include the corresponding incident heat flux, it can be estimated (using the latitude, season, and orientation [ASHRAE 2001]) to be in the range of 350 to 400 W/m². In the CFD results, the brick wall temperature varied from 330 to 345 K, as the wind speed varied from 10 to 4 m/s for a surface heat source of 630 W/m². In order to compare these CFD results to the experimental data, it was necessary to account for the difference in solar heat flux. For steady-state conditions, the difference between the air temperature and the brick temperature is proportional to the absorbed solar energy. Assuming that the air temperature and convection conditions on both sides of the wall remained about the same, the brick temperatures predicted by the model and adjusted for a reduced heat flux of 400 W/m² would range from 320 to 330 K, in good agreement with the experimental data.

Table 3. A Comparison of CFD Results to Empirical Data for Flow through the Ventilation Slots

	Discharge Coefficient (C_d)	Flow Exponent (n)
Empirical data (Straube 1998)	0.626	0.56
CFD, top slot ($R^2=0.99$)	0.640	0.55
CFD, bottom slot ($R^2=0.97$)	0.632	0.55

Table 4. A Comparison of CFD Results to Empirical Data for Total Pressure Drops and Airflow Rates

	Experimental Data	CFD Model
System pressure drop as cavity depth goes from 19 to 50 mm	Unchanged (Piñon et al. 2004)	Unchanged
System mass flow rate as the cavity depth goes from 19 to 50 mm	Unchanged (Piñon et al. 2004)	Unchanged
Air flow rate when ventilation slot height doubled	Doubled (Straube and Burnett, 1998b)	Doubled
Air flow rate in cavity	0.05 to 0.15 m/s for wind speeds from 1 to 3 m/s, unknown geometry Kuenzel and Mayer (1983), as quoted in Straube (2004)	19 mm cavity: 0.06 to 0.11 m/s 50 mm cavity: 0.02 to 0.04 m/s for wind speeds from 0 to 4 m/s
Range of total pressure drops	-1 to 3 Pa over extended field test periods (Straube 1995)	-2 to 7 Pa for wind speeds from 0 to 4 m/s

From the same experimental data, the difference between outdoor air temperature and cavity air temperature ranged between -5 and 22 K over an April to August period (Straube and Burnett 1998b). The comparable CFD results ranged from -1 to 26 K for the summer cases with solar heat fluxes up to 630 W/m².

Pressure and Mass Flow Rate Comparisons

The pressure drop and airflow rates through a brick wall ventilation slot have been measured for a slot size of 11 by 65 by 110 mm (Straube 1998). Straube correlated his experimental data against a general power law expression useful for deep orifices or slots, as shown in Equation 1. Table 3 shows that the CFD results, where the slots had similar dimensions of 9 by 79 by 116 mm, are in close agreement with the empirical results. A comparison of the flow exponents in Table 3 to that expected for a clean-edged circular orifice (0.5 for fully turbulent and 1.0 for laminar) seems to confirm the dominance of turbulence in the slots.

$$\frac{Q}{A} = C_d \left(\frac{2\Delta P}{\rho} \right)^n \quad (1)$$

where

- Q = flow rate, m³/s
- A = area of the orifice, m²
- ρ = mass density of the air, kg/m³
- ΔP = air pressure difference, Pa
- C_d = factor that accounts for friction and turbulence losses
- n = flow exponent

Other experimental results for pressure drop through the slots are presented in the form of a loss factor as shown in Equation 2. This loss factor is also based on the power law form but assumes a value of 0.5 for the flow exponent. Based on experimental results for slots facing still air on the outlet, this report recommends a loss factor of 1.5 (Piñon et al, 2004). The CFD models produce a loss factor of 2.1. The difference is likely due to the model's geometry where air exiting the slot enters a constrained space rather than still air.

$$f = \frac{2\Delta P}{\rho V^2} \quad (2)$$

where

V = velocity, m/s

The CFD results were also compared to experimental results with regard to cavity depth and ventilation slot height variations. A "reasonableness" check on the CFD total pressure drop and cavity velocity results was available for a range of outdoor wind speeds. These comparisons also offer confidence in the CFD model and are summarized in Table 4.

RESULTS

Pressure and Mass Flow Rates

It is helpful to examine an overview of the pressure variations throughout the computational domain, as shown in Figure 4. This figure traces an imaginary air path (shown in side

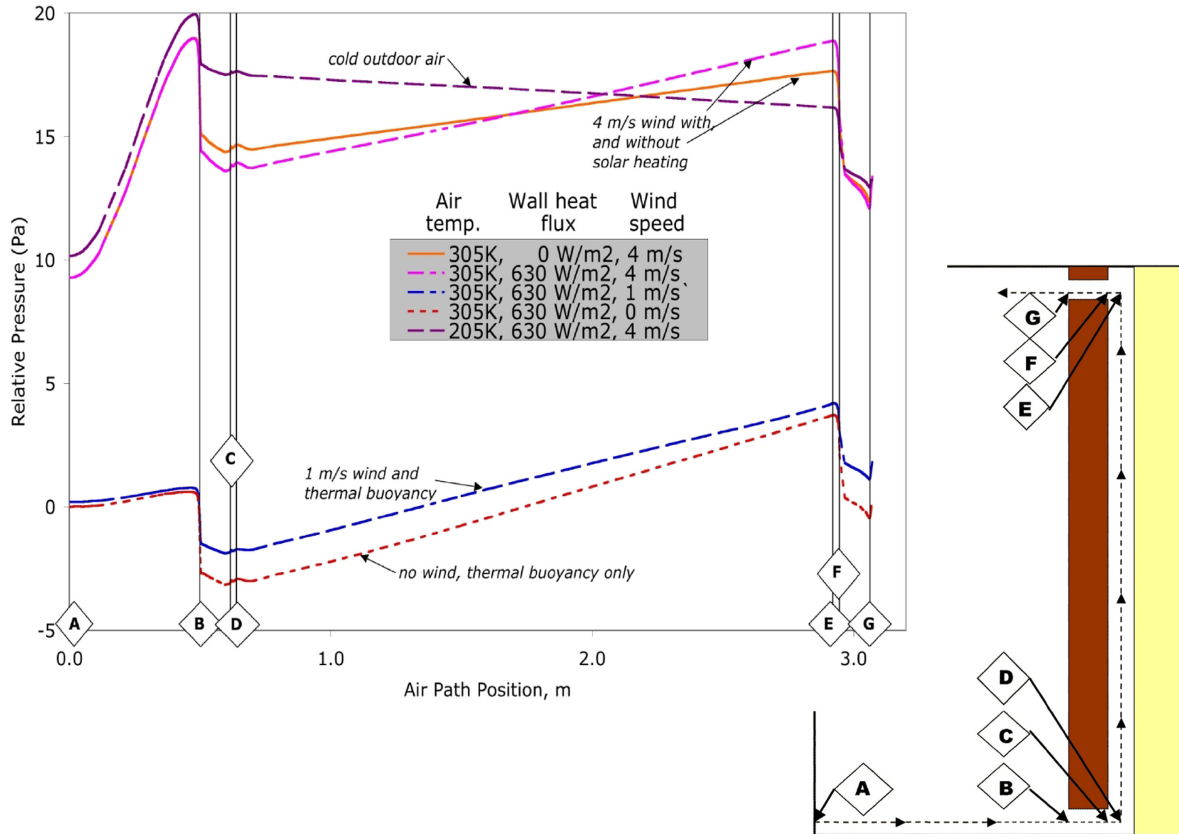


Figure 4 Pressure variation along an imaginary air path flowing through the bottom vent, upward through the cavity, and out the top vent.

view), starting at “A” 0.5 m in front of the wall at a specified temperature and velocity, traveling to “B” at the bottom vent of the brick wall, turning upward at the center of the cavity (at “D”), and exiting the cavity through the top vent (at “G”). The selected cases included in this figure show the relative importance of the inlet wind speed, the heat flux on the outside of the brick wall, and the air temperature. For example, by comparing the two curves that represent an inlet air temperature of 305 K and a wind speed of 4 m/s, it becomes apparent that the pressure profile is only slightly affected by the heat flux on the brick wall surface. For cold outdoor air, the effect of solar heating was even less. In contrast, the pressure profile is greatly affected by the normal wind speed, as is shown by comparing the three cases for no wind, 1 m/s wind, and 4 m/s wind.

The pressure drop through the ventilation slots occurs mainly at the slot entrance (at points “B” and “F”), although there is a small contribution to the overall pressure drop due to friction within the slot itself, as shown in Figure 4. These pressure changes through the constricted openings to the ventilation space are a function of the mass flow rate through the ventilation slots.

The pressure change through the remainder of the cavity (between points “D” and “E” in Figure 4) was very small, ranging from 3 to 6 Pa in the summer and from –2 to 1 Pa in the winter, as shown on Figure 5. Examination of the five cases at a heat flux of 630 W/m² on Figure 5 shows that this pressure drop through the vertical cavity decreases as the outdoor wind speed increases, mainly because the greater wind speeds reduce the brick temperatures.

A number of cases were examined to determine the relative effectiveness of increasing the cavity depth versus increasing the size of the ventilation slot. As Figures 6 and 7 show, there was no significant difference between any of the reported pressure drops or the mass flow rates as the cavity depth varied from 19 to 50 mm. This comparison shows that the resistance of the laminar flow in the cavity was similar in both cases. In contrast, Figure 7 shows that increasing the ventilation slot height from 79 mm to 158 mm doubled the air flow rate from 0.0008 to 0.0016 m³/s·m². This shows that the ventilation slot size provides the main control on the airflow through the cavity.

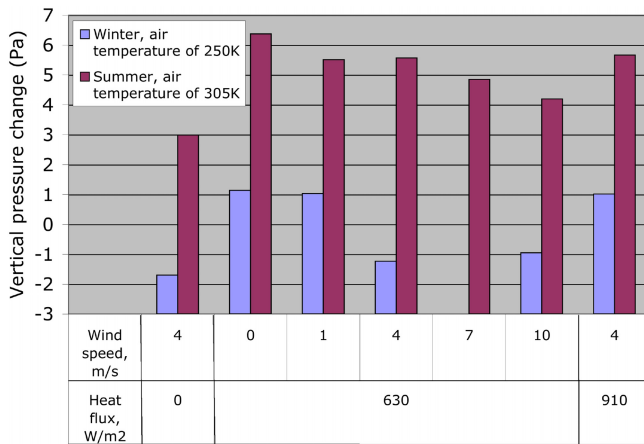


Figure 5 Pressure change through the height of the ventilation cavity.

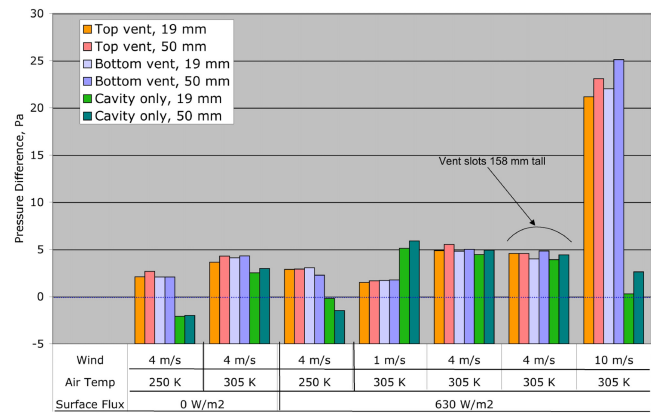


Figure 6 Comparison of pressure drops for ventilation cavities of two depths—19 mm and 50 mm—and two vent sizes (all are 79 mm tall except where indicated).

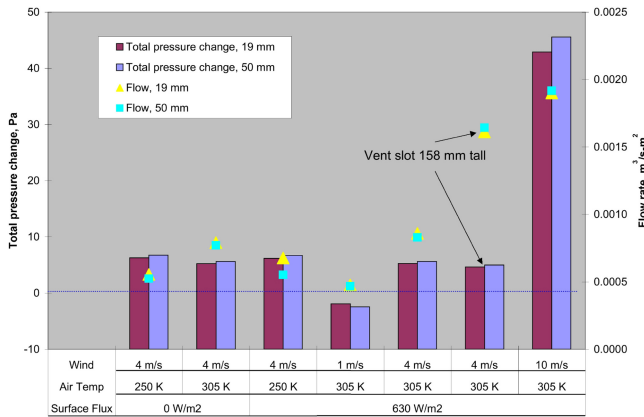


Figure 7 Comparison of total pressure drop and mass flow rate for two cavity depths and two vent sizes (all vents are 79 mm tall except where indicated).

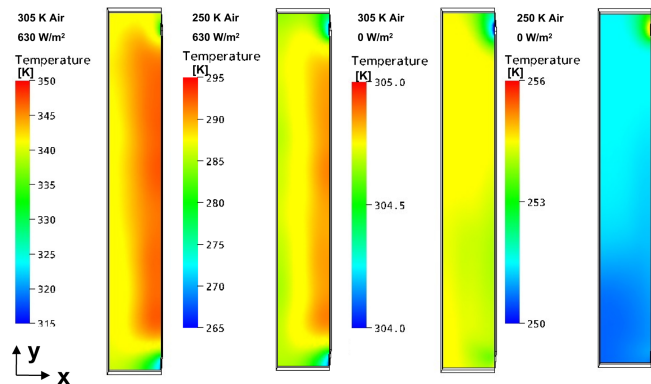


Figure 8 Temperature (K) on the brick face of the 50 mm ventilation cavity with a 4 m/s wind speed for (from left to right): summer day, winter day, summer night, winter night.

Thermal Effects

In one- and two-dimensional hygrothermal models, brick temperature is implicitly considered constant over the face of the wall. This analysis examined the appropriateness of that assumption. The temperature difference from one face of the brick wall to the other was 0–2 K for most of the cases. A maximum difference of 5 K was found for a few of the cases with very low wind speeds. The temperature field on the brick side of the ventilation cavity, shown in Figure 8, was affected chiefly by three factors: whether or not solar heating was present, high heat transfer rates at the bottom and top ventilation slots, and variations in air velocity outside the wall. The temperature profiles for the night (i.e., 0 W/m² heat flux) cases were relatively uniform and came within 1–2 K of the external

air temperature. The temperatures on the brick face in the presence of a strong (630 W/m²) solar heat flux showed more variation, but the variation with height did not change very much, supporting the constant temperature assumption of a one-dimensional hygrothermal model. The horizontal temperature variations, on the order of 2 to 5 K, are an artifact of the selected wind direction and boundary conditions. Because one side of the model was a plane of symmetry, all of the air entering the computational domain normal to the wall was forced to turn either toward the other side or upward. This increased the mass flow rate, air velocity, and heat transfer rates in those areas relative to the region near the symmetry plane. The variation in convective heat transfer over the external surface of a real wall will also be strongly dependent upon the wind direction and other topological features near the house.

Table 5. Coefficients for Equation 3 for Ventilation Cavity Pressure Change and Ventilation Cavity Flow Rate

	C1 (intercept)	C2 ($\sqrt{V_{air}}$)	C3 (V_{air})	C4 (V_{air}^2)	C5 ($1/T_{air}$)	C6 (E_{solar})	C7 (A_R)
Mass Flow, kg/s, adj. R² = 0.99							
Coefficient	8.84E-4	-4.89E-4	2.99E-4	0	-0.338	1.43E-7	4.27
Std. Error	1.5E-4	4.6E-5	1.3E-5		0.036	5E-8	0.22
Mass Flow, kg/s, adj. R² = 0.98							
Coefficient	7.45E-4	0	0	1.57E-5	-0.317		4.58
Std. Error	2.4E-4			6.1E-7	0.06		0.34
Total Pressure Change, Pa, adj. R² = 0.99							
Coefficient	-1.16	0	0	0.459	0	0	0
Std. Error	0.35			8.8E-3			
Pressure Change in Top Vent, Pa, adj. R² = 0.99							
Coefficient	7.82	0	0	0.203	-2170	1.94E-3	0
Std. Error	1.6			4.7E-3	420	5.5E-4	
Pressure Change in Bottom Vent, Pa, adj. R² = 0.98							
Coefficient	8.04	0	0	0.220	-2290	1.82E-3	0
Std. Error	2.2			6.4E-3	580	7.6E-4	

Correlations with Weather Variables

Multivariate regression techniques were used to explore the relationships between external weather and wall geometric variables and the airflow and pressure changes in the ventilation cavity. The multivariate models were defined considering the physics underlying this complex problem. For example, buoyancy forces will be a function of the inverse of the temperatures. The brick temperature will be a function of the air temperature and the square root of the velocity, as well as the surface heat flux. The stagnation pressure (or wind driving force) at the wall will be a function of the square of the velocity.

The results of these regression analyses are summarized in Equation 3 and Table 5. All of the coefficients shown in Table 5 are significant at the 95% confidence level and all of the adjusted regression coefficients were greater than 98%.

$$X = C_1 + C_2\sqrt{V_{air}} + C_3V_{air} + C_4V_{air}^2 + \frac{C_5}{T_{air}} + C_6E_{solar} + C_7A_R \tag{3}$$

where

- X = desired quantity, pressure change, or flow rate
- C_1-C_7 = coefficients determined by multivariate regression (see Table 5)
- V_{air} = wind velocity, normal to wall, m/s
- T_{air} = temperature of the outside environment, K
- E_{solar} = absorbed solar radiation, W/m²
- A_R = vent area per wall area (including top and bottom vents), m²/m²

These correlations apply only to discrete rectangular vents in a thick wall with the wind normal to that wall. In general, they are limited by the scope of the parametric study and other model limitations, including

- no air diffusion through the bricks;
- no air leakage through the interior wall;
- smooth surfaces, no mortar protrusions or blockages;
- no wind perturbations;
- only dry air;
- wind direction normal to the wall; and
- single ventilation geometry with fixed horizontal and vertical spacing between openings, fixed wall height.

The mass flow rate through the ventilation cavity is represented equally well by two equations shown in Table 5, both of which are strongly related to the ventilation opening size. The first is a function of solar radiation, as well as wind velocity, and the inverse of the outdoor air temperature. The second matches the matrix of model results almost as well and is a simpler function of the normal wind velocity squared and the inverse of the outdoor air temperature. These two factors relate directly to the stagnation pressure at the wall surface and the buoyancy force due to the difference between the air temperature outside and that within the cavity.

The total pressure change, from the cavity inlet outside the bottom of the wall to the outlet near the top, is determined solely by the square of the wind speed, i.e., it is a function of the external stagnation pressure.

The pressure changes in the vent slots are really a function of their geometry and the average air velocity in the slot.

Although these pressure changes are given as functions of weather and geometry in Equation 3 and Table 5, it is also possible to use the mass flow rate derived from Equation 3 with the pressure drop relationships shown in Equations 1 or 2.

SUMMARY AND DISCUSSION

A CFD model of a brick rain screen wall was developed to determine useful relationships between weather and wall geometry and the resulting airflow within the ventilation cavity. The model was benchmarked by comparing its results to experimental data for factors, including

- flow field patterns,
- total pressure drop through the cavity,
- pressure drop through the ventilation slots,
- total mass flow through the cavity, and
- thermal conditions at the brick wall.

The parametric study was designed to examine variations in wind speed, solar radiation, cavity depth, vent slot size, and outdoor air temperature. One of the main objectives was to determine whether an increase in cavity depth would increase the airflow through the space. The results of this study found no significant difference in the mass flow rates between cavity depths of 19 and 50 mm. In contrast, doubling the ventilation slot height doubled the airflow rate, showing the ventilation slot size is the controlling factor for the range of cases considered here. (Of course, the greater depth may still be desired to avoid any localized airflow blockages due to protruding mortar.) The effects of natural convection within the air cavities, driven by the temperature difference between the cavity walls and the outside air, also affected the ventilation flow.

Using the CFD results, correlations were produced to estimate the mass flow and pressure drops in the cavity for use in more general transient hygrothermal models, using variables available in typical weather data files. The correlations given here are limited by the scope of the parametric study and the other model limitations, most significantly

- effects of wind direction and perturbation were not modeled,
- a single vent spacing arrangement with discrete pairs of rectangular openings was modeled, and
- additional buoyancy effect of variations in moisture content was not modeled.

More work is needed to explore the effect of varying the horizontal distribution of the ventilation slots in addition to the consideration of increased slot height used here. Future work should also explore the effects of environmental factors outside the wall, such as variations due to wind direction and air blockages (e.g., shrubbery). It would also be helpful to expand the external air volume to include a typical soffit arrangement, which could significantly change the pressure conditions at the exit of the top vent.

REFERENCES

- AEA Technology Engineering Software Ltd, Didcot Oxfordshire, United Kingdom.
- ASHRAE. 2001. *2001 ASHRAE Handbook—Fundamentals*. Atlanta: American Society of Heating, Refrigerating and Air-Conditioning Engineers, Inc.
- Balocco, C. 2001. A simple model to study ventilated facades energy performance. *Energy and Buildings*, Vol. 34, pp. 469-475.
- Burnett, E.F.P., and J.F. Straube. 1995. Vents, ventilation drying, and pressure moderation, Research Report. Canada Mortgage and Housing Corporation.
- Choi, E.C.C., and Z. Wang. 1998. Study on pressure-equalization of curtain wall systems. *Journal of Wind Engineering and Industrial Aerodynamics*, Vol. 73, pp. 251-266.
- Hansen, M., A. Nicolajsen, and B. Stang. 2002. On the influence of ventilation on moisture content in timber framed walls. *Building Physics 2002 6th Nordic Symposium*.
- Karagiozis, A. 2001. Introduction to MOISTURE-EXPERT Software. Oak Ridge National Laboratory, Oak Ridge, Tenn.
- Kays, W.M., and M.E. Crawford. 1980. *Convective Heat and Mass Transfer*. New York: McGraw-Hill.
- Kumar, K.S., T. Stathopoulos, and J.A. Wisse. 2003. Field measurement data of wind loads on rainscreen walls. *Journal of Wind Engineering and Industrial Aerodynamics*, Vol. 91, pp. 1401-1417.
- Kumar, K.S., and J.A. Wisse. 2001. Pressure equalization of rainscreen facades: Analysis of the field data in the frequency domain. *Wind and Structures* 4(2):101-118.
- Künzel, H., and E. Mayer. 1983. Untersuchung über die notwendige Hinterlüftung an Außenwandbekeidung aus großformatigen Bauteilen, *Schriftenreihe Bundesminister für Raumordnung, Bauwesen, und Städtebau*, 3/1983.
- Künzel, H., and E. Mayer. 1984. *Wärme- und Regenschutz bei zweischaligem Sichtmauerwerk mit Kerndämmung*. BMFT-Forschungsbericht T84-191.
- Mayer, E., and H. Künzel. 1983. Untersuchungen über die notwendige Hinterlüftung an Außenwandbekeidung aus großformatigen Bauteilen, Fraunhofer Institut für Bauphysik, *Forschungsbericht B Ho 1/83*, March, 1983.
- Piñon, J., D. Davidovic, E. Burnett, and J. Srebic. 2004. Characterization of ventilation airflow in screened wall systems, ASHRAE 1091 Report #5.
- Popp, W., E. Mayer, and H. Künzel. 1980. Untersuchungen über die Belüftung des Luftraumes hinter vorgesetzten Fassadenbekleidung aus kleinformatischen Elementen, Fraunhofer Institut für Bauphysik, *Forschungsbericht B Ho 22/80*, April, 1980.
- Schwarz, B. 1973. Witterungsbeanspruchung von Hochhausfassaden, *HLH Bd. 24(12):376-384*.
- Shakerin, S., M. Bohn, and R.I. Loehrke. 1988. Natural convection in an enclosure with discreet roughness ele-

- ments on a vertical heated wall. *Int. J. Heat Mass Transfer* 31(7):1423-1430.
- Straube, J.F. 2004. Ventilated wall systems: Review of literature and theory, ASHRAE 1091 Report # 1.
- Straube, J.F., and E.F.P. Burnett. 1998a. Vents, ventilation and masonry veneer wall systems. *Proceedings of the Eighth Canadian Masonry Symposium. Jasper, Alta., Canada*, pp. 194-207.
- Straube, J.F., and E.F.P. Burnett. 1998b. Drainage, ventilation drying, and enclosure performance. *Conference Proceedings, Thermal Performance of The Exterior Envelopes of Buildings VII. Clearwater Beach, Florida*, pp. 189-198.
- Straube, J.F. 1998. Moisture control and enclosure wall systems, Ph.D. dissertation, Civil Engineering Dept., University of Waterloo, UMI Dissertation Services.